CHEMISTRY OF MATERIALS
Article

Chem. Mater. **2010,** *22,* 27–35 27
DOI:10.1021/cm9009767

New Tantalum Amido Complexes with Chelate Ligands as Metalorganic (MO) Precursors for Chemical Vapor Deposition (CVD) of Tantalum Nitride Thin Films

Tianniu Chen,* Chongying Xu, Thomas H. Baum, Gregory T. Stauf, Jeffrey F. Roeder, Antonio G. DiPasquale,† and Arnold L. Rheingold†

Advanced Technology Development Division, Advanced Technology Materials Inc. (ATMI), 7 Commerce Drive, Danbury, Connecticut 06810, †Department of Chemistry and Biochemistry, University of California, San Diego, 9500 Gilman Drive, MC 0358, Urey Hall 5128, La Jolla, CA 92093-0358

Received April 8, 2009. Revised Manuscript Received October 14, 2009

Four new tantalum amido precursors (η^2-RN(CH$_2$)$_n$NR)Ta(NMe$_2$)$_3$ (where R = Me, n = 2, **1**; R = Et, n = 2, **2**; R = Me, n = 3, **3**; R = Et, n = 3, **4**) with chelate diamide ligands and one new tantalum amido precursor (η^2-^{t}BuNC(NMe$_2$)NEt)Ta(NMe$_2$)$_4$) (**5**) with a chelate guanidinate ligand were prepared and characterized. Their thermal behavior, especially (NMe$_2$)$_3$Ta(η^2-MeN(CH$_2$)$_2$NMe) (**1**), were investigated by thermogravimetric analysis (TGA) and differential scanning calorimetry (DSC) experiments to demonstrate the enhancement of their thermal stability and preservation of the volatility as metalorganic chemical vapor deposition (MOCVD) precursors as compared to Ta(NMe$_2$)$_5$ (PDMAT). Introduction of the asymmetric chelate guanidine ligand in complex **5** gave improved volatility as compared with its known isomer [(η^2-^{i}PrNC(NMe$_2$)N^{i}Pr)Ta(NMe$_2$)$_4$ (**6**). The crystal structures of **5** and **6** were measured to investigate the correlation between the volatility and intermolecular interactions. The MOCVD of tantalum nitride thin films was successfully achieved using **1**. The films are based on field emission scanning electron microscopy (FESEM) and show good adhesion properties. Rutherford backscattering spectrometry (RBS) and X-ray photoelectron spectroscopy (XPS) data suggest that the film deposited using **1** at 500 °C under ammonia has a composition of TaN$_{1.22\pm0.14}$ with negligible carbon and oxygen levels. It also shows low resistivity of 1.4×10^3 $\mu\Omega$ cm on SiO$_2$/Si and broad X-ray diffraction (XRD) peaks for the stoichiometric cubic refractory TaN, indicating the potential of **1** becoming an alternative MOCVD precursor for barrier applications.

Introduction

Tantalum nitride (TaNx) films have been an attractive candidate as a diffusion barrier for copper-interconnect technologies because of their high thermal, mechanical, chemical stability, and good electrical conductivity.[1−4] Other important applications include gate electrodes for complementary metal oxide semiconductor (CMOS), as well as electrodes for capacitors used in memory devices.[5,6] More recently, tantalum nitride thin films have also been proposed as barrier layers for 3D integrated all-solid-state rechargeable batteries.[7]

Tantalum nitride films have been deposited by several techniques such as physical vapor deposition (PVD),[1,4,8] chemical vapor deposition (CVD),[9−13] and atomic layer deposition (ALD).[14−19] However, with the continued scaling down of device dimensions in the semiconductor technology now entering the nanoscale regime, the conventional PVD technique will face challenges due to its

*To whom correspondence should be addressed. Tel.: 2037391405. Fax: 2038302123. E-mail: tchen@atmi.com.

(1) Nicolet, M.-A. *Thin Solid Films* **1978**, *52*, 415.
(2) Holloway, K.; Fryer, P. M.; Cabral, C., Jr.; Harper, J. M. E.; Bailey, P. J.; Kelleher, K. H. *J. Appl. Phys.* **1992**, *71*, 5433.
(3) Olowolafe, J. O.; Mogab, C. J. *J. Appl. Phys.* **1992**, *72*, 4099.
(4) Sun, X.; Kolawa, E.; Chen, J.; Reid, J. S.; Nicolet, M.-A. *Thin Solid Films* **1993**, *236*, 347.
(5) Kadoshima, M.; Akiyama, K.; Yamamoto, K.; Fujiwara, H.; Yasuda, T.; Nabatame, T.; Toriumi, A. *J. Vac. Sci. Technol. B* **2005**, *23*, 42.
(6) Kingon, A. I.; Maria, J.; Streiffer, S. K. *Nature* **2000**, *406*, 1032.
(7) Knoops, H. C. M.; Baggetto, L.; Langereis, E.; van de Sanden, M. C. M.; Klootwijk, J. H.; Roozeboom, F.; Niessen, R. A. H.; Notten, P. H. L.; Kessels, W. M. M. *J. Electrochem. Soc.* **2008**, *155*, G287.
(8) Li, N.; Ruzic, D. N.; Powell, R. A. *J. Vac. Sci. Technol. B* **2004**, *22*, 2734.
(9) Fix, R.; Gordon, R. G.; Hoffman, D. M. *Chem. Mater.* **1993**, *5*, 614.
(10) Lehn, M. J.; Heide, P. V. D.; Wang, Y.; Suh, S.; Hoffman, D. M. *J. Mater. Chem.* **2004**, *14*, 3239.
(11) Newport, A. C.; Bleau, J. E.; Carmalt, C. J.; Parkin, I. P.; O'Neill, S. A. *J. Mater. Chem.* **2004**, *14*, 3333.
(12) Tsai, M. H.; Sun, S. C.; Chiu, H. T.; Tsai, C. E.; Chuang, S. H. *Appl. Phys. Lett.* **1995**, *67*, 1128.
(13) Rische, D.; Parala, H.; Baunemann, A.; Thiede, T.; Fischer, R. *Surf. Coat. Technol.* **2007**, *201*, 9125.
(14) Kim, H.; Detavenier, C.; van der Straten, O.; Rossnagel, S. M.; Kellock, A. J.; Park, D.-G. *J. Appl. Phys.* **2005**, *98*, 014308.
(15) Park, J.; Lee, M.; Lee, C.; Kang, S. *Electrochem. Solid-State Lett.* **2001**, *4*, C17.
(16) Kim, H.; Kellock, A. J.; Rossnagel *J. Appl. Phys.* **2002**, *92*, 7080.
(17) Park, J.; Park, H.; Kang, S. *J. Electrochem. Soc.* **2002**, *149*, C28.
(18) Kim, H. *J. Vac. Sci. Technol. B* **2003**, *21*, 2231.
(19) Knoops, H. C. M.; Baggetto, L.; Langereis, E.; van de Sanden, M. C. M.; Klootwijk, J. H.; Roozeboom, F.; Niessen, R. A. H.; Notten, P. H. L.; Kessels, W. M. M. *ECS Trans.* **2007**, *11*, 45.

Published on Web 11/25/2009

limited conformality. As a result, CVD or ALD processes are required for growing conformal thin films with good step coverage and accurate control of film thickness and composition on aggressive device geometries in CMOS applications. The availability of precursors with appropriate properties such as high purity, high volatility, and high thermal stability is needed to enable CVD or ALD processes that produce high quality thin films. The commonly used CVD precursors for growing tantalum nitride films include halides and MO precursors. Although tantalum halides are readily available and tend to exhibit simple deposition chemistry, they are intrinsically less volatile, require higher deposition temperatures to achieve films with low halogen impurities, and release corrosive hydrogen halide vapor as compared to MO precursors.[11,20] On the other hand, homoleptic tantalum alkylamides such as $Ta(NMe_2)_5$ (PDMAT),[9,19,21−23] $Ta(NMeEt)_5$ (PEMAT),[24−26] and $Ta(NEt_2)_5$ (PDEAT)[27−29] have been the most widely used MO precursors for CVD of TaNx, but they have limited thermal stability and are highly sensitive to air and moisture.

A general chemical approach for improving thermal stability and maintaining the volatility of a precursor is by introducing chelating ligands. This approach has been demonstrated to improve the thermal stability of metal alkoxide and amide complexes of Ta and Nb using monoanionic chelate β-diketonate and ketoiminate ligands for growing metal oxide films in an MOCVD mode.[30−33] However, the modification of chemistry of homoleptic tantalum amido complexes with only nitrogen-coordinated chelate ligands and their applications in MOCVD processes has remained limited only to guanidinato/amidonato,[13,34−40] hydrazido,[41] diamido pyridine/amine,[42,43] and amido/amine complexes.[44]

Scheme 1. Synthesis of Tantalum Diamido Complexes (η^2-$R^1N(CH_2)_nNR^2$)$Ta(NMe_2)_3$ (1−4) and Tantalum Amido/Guanidinato Precursor [(η^2-^{t}BuNC(NMe_2)NEt)$Ta(NMe_2)_4$)] (5) and [(η^2-^{i}PrNC(NMe_2)N^{i}Pr)$Ta(NMe_2)_4$] (6)[34]

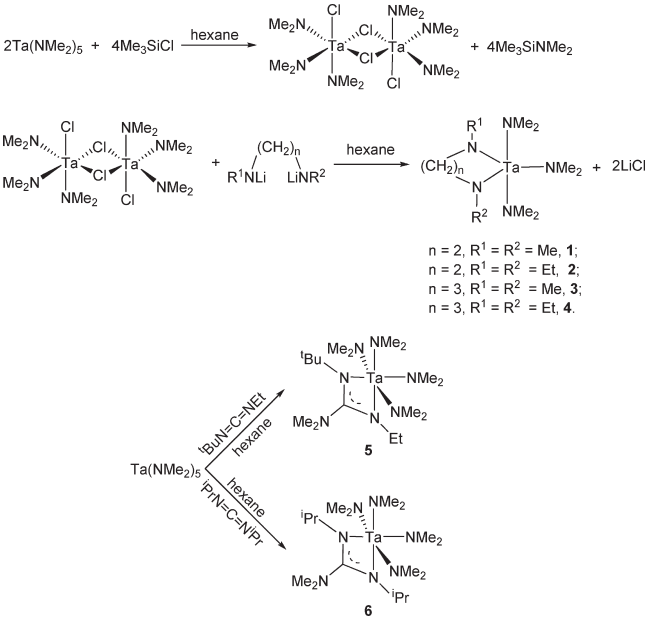

Herein for the first time, we report the syntheses and characterization of a family of mixed amido tantalum complexes with diamido chelate ligands (η^2-RN-$(CH_2)_n$NR)$Ta(NMe_2)_3$ (where R = Me, n = 2, **1**; R = Et, n = 2, **2**; R = Me, n = 3, **3**; R = Et, n = 3, **4**) (Scheme 1). We also explored an alternative route of introducing chelate ligands by incorporating the carbodiimide moiety to PDMAT and obtained a new amido/guanidinato precursor [(η^2-^{t}BuNC(NMe_2)NEt)$Ta(NMe_2)_4$)] (**5**) (Scheme 1). The crystal structure of **5** and its isomer [(η^2-^{i}PrNC-(NMe_2)N^{i}Pr)$Ta(NMe_2)_4$] (**6**)[34] were determined to study ligand effects. The thermal properties of complexes **1**−**6** were measured by simultaneous thermal analyses (STA) including thermogravimetric analysis (TGA) and differential scanning calorimetry (DSC). Isothermal TGA experiments were performed on diamide complexes **1** and guanidinate **5**, which exhibit the best thermal behavior within their classes, respectively, when compared to the widely used PDMAT, to show their enhanced thermal stabilities and relative volatilities. The better of the two, complex **1,** was employed for MOCVD of tantalum nitride films and referenced to PDMAT to demonstrate its advantages as an alternative CVD precursor.

(20) Bleau, J. E.; Carmalt, C. J.; O'Neill, S. A.; Parkin, I. P.; White, A. J. P.; Williams, D. J. *Polyhedron* **2005**, *24*, 463.
(21) Bradley, D. C.; Thomas, I. M. *Can. J. Chem.* **1962**, *40*, 1355.
(22) Riley, P. N.; Parker, J. R.; Fanwick, P. E.; Rothwell, I. P. *Organometallics* **1999**, *18*, 3579.
(23) Engbrecht, E. R.; Sun, Y.; Smith, S.; Pfiefer, K.; Bennett, J.; White, J. M.; Ekerdt, J. G. *Thin Solid Films* **2002**, *418*, 145.
(24) Bhandari, G.; Baum, T. H. Tantalum amide precursors for deposition of tantalum nitride on a substrate. U.S. Patent 6,015,917, Jan 18, **2000**.
(25) Bhandari, G.; Baum, T. H. Tantalum amide precursors for deposition of tantalum nitride on a substrate. U.S. Patent 6,379,748, Apr 30, **2002**.
(26) Bilodeau, S. M.; Vestyck, D. J.; Ragaglia, C.; Stauf, G. T.; Roeder, J. F.; Baum, T. H. Process and thin film characteristics of TaN deposited by MOCVD. Proceedings of the Advanced Metallization Conference; Montreal, Canada, Oct 8−11, 2001.
(27) Im, S.; Kim, S.; Park, K.; Cho, S.; Kim, K. *Mater. Res. Soc. Symp. Proc.* **2000**, *612*, D 6.7.1.
(28) Chiu, H.; Chang, W. *J. Mater. Sci. Lett.* **1992**, *11*, 96.
(29) Davies, H. O.; Jones, A. C.; McKinnell, E. A.; Raftery, J.; Muryn, C. A.; Afzaal, M.; O'Brien, P. *J. Mater. Chem.* **2006**, *16*, 2226.
(30) Pollard, K. D.; Puddephatt, R. J. *Chem. Mater.* **1999**, *11*, 1069.
(31) Lim, S.; Lee, J.; Sohn, D. S.; Lee, W. I.; Lee, I. *Chem. Mater.* **2002**, *14*, 1548.
(32) Williams, P. A.; Jones, A. C.; Wright, P. J.; Crosbie, M. J.; Bickley, J. F.; Steiner, A.; Davies, H. O.; Leedham, T. J. *Chem. Vap. Deposition* **2002**, *8*, 110.
(33) Hellwig, M.; Milanov, A.; Barecca, D.; Deborde, J.; Thomas, R.; Winter, M.; Kunze, U.; Fischer, R. A.; Devi, A. *Chem. Mater.* **2007**, *19*, 6077.
(34) Tin, M. K. T.; Yap, G. P. A.; Richeson, D. S. *Inorg. Chem.* **1999**, *38*, 998.
(35) Thirupathi, N.; Yap, G. P. A.; Richeson, D. S. *Organometallics* **2000**, *19*, 2573.
(36) Baunemann, A.; Rische, D.; Milanov, A.; Kim, Y.; Winter, M.; Gemel, C; Fischer, R. A. *Dalton Trans.* **2005**, 3051.
(37) Baunemann, A.; Winter, M.; Csapek, K.; Gemel, C.; Fischer, R. A. *Eur. J. Inorg. Chem.* **2006**, 4665.
(38) Heeg, M. J.; Winter, C. H. *Inorg. Chem.* **2009**, *48*, 5382.
(39) Tin, M. K. T.; Yap, G. P. A.; Richeson, D. S. *Inorg. Chem.* **1998**, *37*, 6728.
(40) Tin, M. K. T.; Yap, G. P. A.; Richeson, D. S. *Dalton* **1999**, 2947.
(41) Baunemann, A.; Kim, Y.; Winter, M.; Fischer, R. A. *Dalton Trans.* **2006**, 121.
(42) Gade, L. H.; Mountford, P. *Coord. Chem. Rev.* **2001**, *216−217*, 65.
(43) Pugh, S. M.; Trosch, D. J. M.; Skinner, M. E. G.; Gade, L. H.; Mountford, P. *Organometallics* **2001**, *20*, 3531.
(44) Zhang, X.; Chen, S.; Cai, H.; Im, H.; Chen, T.; Yu, X.; Chen, X.; Lin, Z.; Wu, Y.; Xue, Z. *Organometallics* **2008**, *27*, 1338.

Table 1. Crystal Data and Structure Refinements for (η^2-^{t}BuNC(NMe$_2$)NEt)Ta(NMe$_2$)$_4$ (5) and (η^2-^{i}PrNC(NMe$_2$)N^{i}Pr)Ta(NMe$_2$)$_4$ (6)

	5	6
empirical formula	$C_{17}H_{44}N_7Ta$	$C_{17}H_{44}N_7Ta$
molecular weight	527.54	527.54
temperature (K)	100(2)	100(2)
wavelength Mo Kα (Å)	0.71073	0.71073
crystal size(mm)	0.30 × 0.20 × 0.20	0.40 × 0.30 × 0.30
crystal system, space group	monoclinic, *P*2(1)/*n*	tetragonal, *P*4(2)/*mbc*
a (Å)	11.2064(7)	17.835(2)
b (Å)	14.4508(9)	17.835(2)
c (Å)	14.4693(9)	14.457(2)
α (deg)	90	90
β (deg)	99.5160(10)	90
γ (deg)	90	90
cell volume (Å^3)/*Z*	2310.9(2)/4	4598.9(10)/8
density δ_{calc} (g/cm^{-3})	1.516	1.524
absorption coefficient μ (mm^{-1})	4.770	4.794
F(000)	1072	2144
θ range for data collection (deg)	2.10−28.21	2.10−28.22
completeness to θ = 28.2° [%]	97.3	99.8
index ranges	$-14 \le h \le 14, -18 \le k \le 18, -18 \le l \le 19$	$-22 \le h \le 23, -23 \le k \le 22, -18 \le l \le 18$
reflections collected/unique [*R*(int)]	19582/5357 [*R*(int) = 0.0201]	36812/2830 [*R*(int) = 0.0558]
refinement method	full-matrix least-squares on F^2	full-matrix least-squares on F^2
data/restraints/parameters	5357/0/226	2830/2/139
goodness-of-fit on F^2 (GOF)	1.037	1.097
final *R* indices [$I > 2\sigma(I)$]	R_1 = 0.0240, wR_2 = 0.0623	R_1 = 0.0422, wR_2 = 0.1045
R indices (all data)	R_1 = 0.0257, wR_2 = 0.0633	R_1 = 0.0530, wR_2 = 0.1115
largest difference peak and hole (e Å^{-3})	0.825 and −0.866	1.936 and −1.075

Experimental Section

All manipulations, unless otherwise noted, were performed under a dry nitrogen atmosphere with use of either a drybox or standard Schlenk techniques. Benzene-d_6 was used as received. One dimensional ^{1}H NMR spectra, unless noted, were recorded at 21 °C on a Mercury 300 MHz Fourier transform (FT) spectrometer and referenced to solvents (residual protons in the ^{1}H spectra). ^{n}BuLi in hexanes (1.6 M), HMeN(CH$_2$)$_2$NMeH, HEtN(CH$_2$)$_2$NEtH, HMeN(CH$_2$)$_3$NMeH, HEtN(CH$_2$)$_3$NEtH, ClSiMe$_3$, TaCl$_5$, ^{i}PrN=C=N^{i}Pr, ^{t}BuN=C=NEt, PDMAT, hexanes, and pentane were all purchased from Aldrich and used as received. (NMe$_2$)$_4$Ta(η^2-^{i}PrNC(NMe$_2$)N^{i}Pr) (**6**) and [(NMe$_2$)$_3$TaCl$_2$]$_2$ were prepared according to the reported procedure.[34,45] Elemental analyses were performed by Complete Analysis Laboratories Inc., E&R Microanalytical Division, Parsippany, NJ 07054-4909. STA data were obtained on a Netzsch STA449C instrument in nitrogen atmosphere inside a drybox with argon as a carrier gas. The measurements were performed in open Pt/Rh crucibles with 5−15 mg of sample, the temperature ramp rate was 10 K/min. Crystallographic data (Table 1) for the structures reported in this paper have been deposited with the Cambridge Crystallographic Data Center (CCDC, 12 Union Road, Cambridge CB2 1EZ (UK). Tel.: (+44)1223-336-408. Fax: (+44)1223-336-033. E-mail: deposit@ccdc.cam.ac.uk) as supplementary publication nos. CCDC-716596 and -716597.

Due to the similarities of preparing compounds **1**−**4**, only a detailed synthetic procedure for **1** is described here.

***η^2-N,N′*-Dimethylethylenediamino-tris-dimethylaminotantalum-(η^2-MeN(CH$_2$)$_2$NMe)Ta(NMe$_2$)$_3$ (1).** To a 100 mL Schlenk flask immersed in an ice bath and charged with *N*,*N*′-dimethylethylenediamine (1.11 g, 13.0 mmol) in 50 mL hexanes, 1.6 M *n*-butyl lithium (15.8 mL, 25.3 mmol) was added. A white precipitate appeared after the addition started, and the reaction was exothermic. The reaction mixture comprising MeNLi(CH$_2$)$_2$LiNMe was allowed to warm to room temperature. Next, the MeNLi(CH$_2$)$_2$LiNMe mixture was added dropwise to [(Me$_2$N)$_3$TaCl$_2$]$_2$ (4.39 g, 5.71 mmol) in 100 mL hexanes at room temperature and stirred overnight. Following filtration, the dark brown filtrate was recovered. The volatiles from the filtrate were removed in vacuo at room temperature followed by vacuum distillation at 79 °C and 50 mtorr to yield red orange solid (η^2-MeN(CH$_2$)$_2$NMe)Ta(NMe$_2$)$_3$ (3.06 g, 7.66 mmol, 58.9% yield, mp 39.0 °C). Data for (η^2-MeN(CH$_2$)$_2$NMe)Ta(NMe$_2$)$_3$: ^{1}H NMR (benzene-d_6, 21 °C) δ 3.85 (s, 4H, CH$_3$N(C*H*$_2$)$_2$−); 3.33 (s, 6H, C*H*$_3$N−); 3.24 (s, 18H, (C*H*$_3$)$_2$N−). ^{13}C NMR (benzene-d_6, 21 °C) δ 62.20 (CH$_3$N(*C*H$_2$)$_2$−); 45.36 ((*C*H$_3$)$_2$N−); 44.33 (*C*H$_3$NCH$_2$−). Anal. calcd for TaC$_{10}$H$_{28}$N$_5$: C, 30.08; H, 7.07; N, 17.54. Found: C, 29.89; H, 6.94; N, 17.52.

***η^2-N,N′*-Diethylethylenediamino-tris-dimethylaminotantalum-(η^2-EtN(CH$_2$)$_2$NEt)Ta(NMe$_2$)$_3$ (2).** *N*,*N*′-Diethylethylenediamine (1.11 g, 11.0 mmol) in 100 mL hexanes and *n*-butyl lithium (13.4 mL, 21.4 mmol) were used to generate EtNLi(CH$_2$)$_2$LiNEt *in situ* before the addition of [(MeN)$_3$TaCl$_2$]$_2$ (4.14 g, 5.39 mmol). The volatiles from the filtrate were removed in vacuo at room temperature followed by vacuum distillation at 77 °C and 65 mtorr to yield golden yellow liquid (η^2-EtN(CH$_2$)$_2$NEt)Ta(NMe$_2$)$_3$ (2.01 g, 4.70 mmol, 42.7% yield). Data for (η^2-EtN(CH$_2$)$_2$NEt)Ta(NMe$_2$)$_3$: ^{1}H NMR (benzene-d_6, 21 °C) δ 3.80 (s, 4H, CH$_3$CH$_2$N(C*H*$_2$)$_2$−); 3.52 (q, 4H, CH$_3$*C*H$_2$N−); 3.22 (s, 18H, (C*H*$_3$)$_2$N−); 1.17(t, 6H, *C*H$_3$CH$_2$N−). ^{13}C NMR (benzene-d_6, 21 °C) δ 58.54 (CH$_3$CH$_2$N(*C*H$_2$)$_2$−); 51.76 (CH$_3$*C*H$_2$NCH$_2$−); 45.51 ((*C*H$_3$)$_2$N−); 17.80 (*C*H$_3$CH$_2$NCH$_2$−). Anal. calcd for TaC$_{12}$H$_{32}$N$_5$: C, 33.71; H, 7.55; N, 16.39. Found: C, 33.42; H, 7.46; N, 16.22.

***η^2-N,N′*-Dimethylpropanediamino-tris-dimethylaminotantalum-(η^2-MeN(CH$_2$)$_3$NMe)Ta(NMe$_2$)$_3$ (3).** *N*,*N*′-Dimethylpropanediamine (1.34 g, 13.0 mol) in 100 mL hexanes and *n*-butyl lithium (16.4 mL, 26.2 mmol) were used to *in situ* generate EtNLi(CH$_2$)$_2$LiNEt before the addition of [(MeN)$_3$TaCl$_2$]$_2$ (5.02 g, 6.54 mmol). The volatiles from the filtrate were removed in vacuo at room temperature followed by sublimation at 85 °C and 50 mtorr to yield yellow orange solid (η^2-MeN(CH$_2$)$_3$NMe)Ta(NMe$_2$)$_3$ (2.05 g,

(45) Chisholm, M. H.; Huffman, J. C.; Tan, L. *Inorg. Chem.* **1981**, *20*, 1859.

4.96 mmol, 38.2% yield, mp 64.1 °C). Data for (η^2-MeN-$(CH_2)_3$NMe)Ta$(NMe_2)_3$: ^{1}H NMR (benzene-d_6, 21 °C) δ 3.44 (m, br., 4H, CH_3NCH_2−); 3.26 (s, 18H, $(CH_3)_2N$−), 3.22 (s, 6H, CH_3NCH_2−); 1.85 (m, 2H, $CH_3NCH_2CH_2$−). ^{13}C NMR (benzene-d_6, 21 °C) δ 58.24 (CH_3NCH_2−); 45.77 ($(CH_3)_2N$−); 44.76 (CH_3NCH_2−); 31.99 ($CH_3NCH_2CH_2$). Anal. calcd for $TaC_{11}H_{30}N_5$: C, 31.96; H, 7.32; N, 16.94. Found: C, 31.74; H, 7.46; N, 16.82.

η^2-*N*,*N*′-Diethylpropanediamino-tris-dimethylaminotantalum-(η^2-EtN$(CH_2)_3$NEt)Ta$(NMe_2)_3$ (4). To a *N*,*N*′-diethylpropanediamine (1.72 g, 13.0 mol) in 100 mL hexanes and *n*-butyl lithium (16.5 mL, 26.4 mmol) were used to *in situ* generate EtNLi-$(CH_2)_2$LiNEt before the addition of $[(MeN)_3TaCl_2]_2$ (5.06 g, 6.59 mmol). The volatiles from the filtrate were removed in vacuo at room temperature followed by vacuum distillation at 68 °C and 110 mtorr to yield yellow liquid (η^2-EtN$(CH_2)_3$N-Et)Ta$(NMe_2)_3$ (1.05 g, 2.38 mmol, 18.3% yield). Data for (η^2-EtN$(CH_2)_3$NEt)Ta$(NMe_2)_3$: ^{1}H NMR (benzene-d_6, 21 °C) δ 3.52 (q, br., 4H, $CH_3CH_2NCH_2$−); 3.38 (m, 4H, $CH_3CH_2NCH_2$−), 3.18 (m, 18H, CH_3N−); 1.88 (m, 2H, $CH_3CH_2NCH_2CH_2$−); 1.10 (m, 6H, $CH_3CH_2NCH_2$−). ^{13}C NMR (benzene-d_6, 21 °C) δ 54.61 ($CH_3CH_2NCH_2$−); 53.17 ($CH_3CH_2NCH_2$−); 44.81 ($(CH_3)_2N$−); 33.15 ($CH_3CH_2NCH_2CH_2$−); 18.00 ($CH_3CH_2NCH_2$−). Anal. calcd for $TaC_{13}H_{34}N_5$: C, 35.37; H, 7.76; N, 15.87. Found: C, 35.50; H, 7.66; N, 15.65.

(η^2-^{t}BuNC(NMe_2)NEt)Ta$(NMe_2)_4$ (5). To a 250 mL flask filled with 1-*tert*-butyl-3-ethylcarbodiimide (^{t}BuN=C=NEt) (1.16 g, 9.19 mol) and 100 mL hexanes, PDMAT ($Ta(NMe_2)_5$) (3.73 g, 9.29 mmol) was added at 0 °C. The green−yellow reaction mixture was stirred and warmed up during overnight. All the volatiles were then removed under vacuum. The resulting bright yellow solid was sublimed under vacuum (100 °C, 100 mtorr) to yield yellow solid (^{t}BuNC(NMe_2)NEt)Ta$(NMe_2)_4$ (3.40 g, 6.44 mol, 70.0% overall yield, mp 66.7 °C). Data for (^{t}BuNC(NMe_2)NEt)Ta$(NMe_2)_4$: ^{1}H NMR (benzene-d_6, 21 °C) δ 1.19 (t, 3H, NCH_2CH_3); 1.38 (s, 9H, $NC(CH_3)_3$); 2.47 (s, 6H, $CN(CH_3)_2$); 3.25 (q, 2H, NCH_2CH_3); 3.49 (m, 24H, $N(CH_3)_2$) . ^{13}C NMR (benzene-d_6, 21 °C): δ 168.55 ($CN(CH_3)_2$); 51.36 ($CN(CH_3)_2$); 42.19 ($NC(CH_3)_3$); 47.30 ($N(CH_3)_2$); 40.17 ($NC(CH_3)_3$); 32.17 (NCH_2CH_3); 18.18 (NCH_2CH_3). Anal. calcd for $TaC_{17}H_{44}N_7$: C, 38.71; H, 8.41; N, 18.59. Found: C, 38.55 ; H, 8.50 ; N, 18.26.

MOCVD of 1 and PDMAT. Details of the reactor used to deposit the tantalum nitride films described in this paper have been discussed elsewhere.[46] A Varian-built low pressure MOCVD "warm wall" reactor with 200-mm wafer capability and a load lock was used for tantalum nitride deposition. The load lock provides good control of the substrate/TaNx growth interface and also allows wafers to be loaded directly onto the preheated susceptor, minimizing heat up time. Platen temperatures were measured via a multithermocouple equipped wafer and calibrated vs heater set points and were uniform across the wafer to within ~10 °C. An ATMI-designed flash vaporizer was attached, and the precursor, dissolved in organic solvents was metered into a hot zone where it was quickly vaporized, allowing precise control over the amount of precursor delivered to the system. Precursors and coreactants were mixed in a baffle region above a showerhead before reaching the substrate. Both **1** and PDMAT were dissolved in toluene for delivery to the flash vaporization system mentioned above. Substrates were 6 in. Si, with 1000−5000 Å thermal SiO_2 on top. A Rigaku 3613 wavelength dispersive X-ray fluorescence (XRF) spectrometer was used for thickness analysis of thin films. This tool is not capable of measuring Ta/N ratio or other light elements present in films. Resistivity measurements were made on a Resmap automated 4-point probe station. The typical MOCVD deposition conditions for growth of tantalum nitride thin films are summarized in Table 2. A field emission scanning electron microscope (FESEM, Hitachi S4700) was used to further characterize the surface morphology of the Ta nitride films. XRD data was collected with a Rigaku SmartLab X-ray diffractometer equipped with a Cu source (λ (Kα1) = 1.5406 Å). The tape used in an American Society for Testing and Materials (ASTM) standard adhesion test was purchased from Paul N. Gardner Company, Inc., Pompano Beach, FL. RBS spectra using a 2.275 MeV He^{2+} beam were acquired at a backscattering angle of 160° with an appropriate grazing angle (with the sample oriented perpendicular to the incident ion beam) on a NEC Pelletron (3SDH) by Evans Analytical Group, Sunnyvale, CA, and XPS experiments were carried out by using a PHI Quantum 2000 system equipped with an Al X-ray source (k_α = 1486.6 eV) and a 4 keV Ar^+ sputter gun with a sputter rate at 100 Å/min (SiO_2 equivalent) by Evans Analytical Group, East Windsor, NJ.

Table 2. Deposition Conditions for MOCVD of Tantalum Nitride Thin Films Using 1 and PDMAT

substrate	SiO_2/Si
Ta precursor injection rate	30−60 μmol/min
deposition time	240−960 s
He carrier (vaporizer)	500−1000 sccm
H_2 flow rate	200−1000 sccm
NH_3 flow rate	100−200 sccm

Results and Discussion

Precursor Synthesis, Spectroscopic, and Structural Characterization. The synthetic approaches involve the salt elimination reaction of 1 molar equiv of *in situ* generated lithium salts ($R^1N(CH_2)_nNR^2)Li_2$ with 1 molar equiv of $Ta(NMe_2)_3Cl_2$ in hexanes for diamido complexes **1**−**4** (Scheme 1) and direct insertion of carbodiimides into the Ta−N bond of PDMAT stoichiometrically for tantalum amido/guanidinato precursors **5** and **6** (Scheme 1). Both types of reactions proceed easily under benign conditions. All diamido complexes were purified further through either vacuum distillation or sublimation while pure amido/guanidinato precursors **5** and **6** were collected by sublimation under vacuum. Among these precursors, $(NMe_2)_3Ta(\eta^2$-MeN$(CH_2)_2$NMe) is a low-melting solid (mp 39 °C) and both $(NMe_2)_3Ta(\eta^2$-EtN-$(CH_2)_2$NEt) (**2**) and $(NMe_2)_3Ta(\eta^2$-EtN$(CH_2)_3$NEt) (**4**) are liquid at room temperature. Both (η^2-^{t}BuNC(NMe_2)-NEt)Ta$(NMe_2)_4$ (**5**) and (η^2-^{i}PrNC(NMe_2)N^{i}Pr)Ta$(NMe_2)_4$ (**6**) were recrystallized out of pentane at −30 °C for structural determination. Furthermore, both elemental analysis and NMR spectra of **1**−**5** are consistent with the proposed/measured monomeric structures.

The single-crystal X-ray diffraction results (Figures 1 and 2) confirm the monomeric nature of compound **5** and its highly disordered isomer **6,** and reveal distorted octahedral coordination geometries for tantalum centers with two nitrogens (N5 and N6 in **5**, N1 and N1A in **6**) from the chelate guanidinate ligands and two nitrogens (N2 and

(46) Kirlin, P. S.; Bilodeau, S. M.; van.Buskirk, P. C. *Integr. Ferroelectr.* **1995**, *7*, 307.

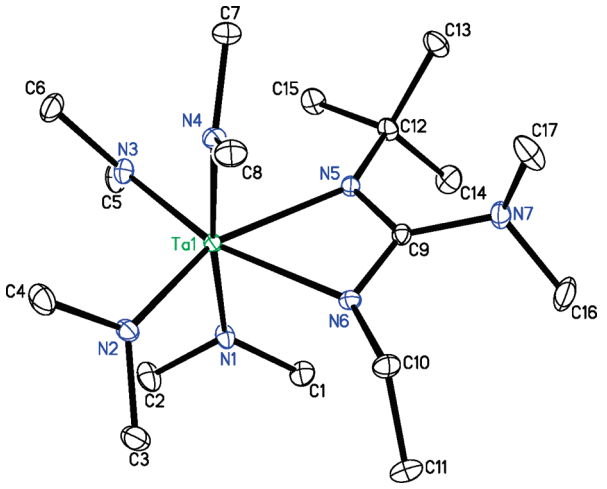

Figure 1. ORTEP diagram of **5** showing 30% thermal ellipsoids. Selected bond lengths [Å] and angles [deg]: Ta(1)−N(1) 2.037(3), Ta(1)−N(2) 2.016(3), Ta(1)−N(3) 2.019(3), Ta(1)−N(4) 2.038(3), Ta(1)−N(5) 2.268(3), Ta(1)−N(6) 2.235(3), C(9)−N(7) 1.425(4), N(1)−Ta(1)−N(3) 92.69(12), N(2)−Ta(1)−N(3) 104.11(12), N(2)−Ta(1)−N(6) 92.94(11), N(3)−Ta(1)−N(5) 104.60(11), N(2)−Ta(1)−N(4) 89.84 (11), N(1)−Ta(1)−N(4) 174.01(11), N(5)−Ta(1)−N(6) 58.31(9).

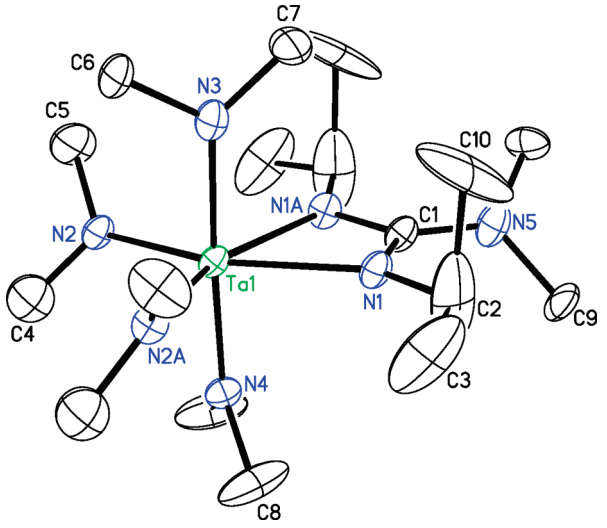

Figure 2. ORTEP diagram of **6** showing 30% thermal ellipsoids. Selected bond lengths [Å] and angles [deg]: Ta(1)−N(1) 2.231(5), Ta(1)−N(2) 2.032(5), Ta(1)−N(3) 2.035(9), Ta(1)−N(4) 2.029(8), C(1)−N(5) 1.381(13), N(1)−Ta(1)−N(4) 89.7(2), N(1)−Ta(1)−N(2A) 99.3(2), N(2)−Ta(1)−N(2A) 102.7 (3), N(2)−Ta(1)−N(3) 91.4(2), N(2)−Ta(1)−N(1A) 99.3(2), N(3)−Ta(1)−N(4) 177.0(3), N(1)−Ta(1)−N(1A) 58.8(3).

N3 in **5**, N2 and N2A in **6**) from dimethylamido groups sitting on the equatorial positions. The guanidinate ligand has restricted bite angles being 58.31(9)° (N(5)—Ta(1)—N(6)) in **5** and 58.8(3)° (N(1)—Ta(1)—N(1A)) in **6**, which are in line with the reported angles (cf. 58.66(14)° in (η^2-CyNC(NMe$_2$)NCy)Ta(NMe$_2$)$_4$,[34] 58.38(19)° in (η^2-^{i}PrNC(^{i}PrN(SiMe$_3$))N^{i}Pr)Ta(NMe$_2$)$_3$(CH$_2$Ph),[35] 59.56(18)° and 58.92(16)° in [(η^2-^{i}PrNC(NMe$_2$)N^{i}Pr)]$_2$Ta(NMe$_2$)(=N^{t}Bu),[36] and 58.4(5)° in [Ta(NEt$_2$)Cl$_3$($^2\eta$-C$_6$H$_5$NC{(C=NC$_6$H$_5$)(HN^{t}Bu)}(N^{t}Bu)][47]). Another set of nitrogens (N1 and N4 in **5**, N3 and N4 in **6**) from two separate dimethylamido ligands occupy the axial positions and are almost linear with the tantalum centers (∠N(1)—Ta(1)—N(4) being 174.01(11)° in **5** and ∠N(3)—Ta(1)—N(4) being 177.0(3)° in **6**), which are also consistent with the corresponding angles in the literature (177.3(2)° in (η^2-CyNC(NMe$_2$)NCy)Ta(NMe$_2$)$_4$,[34] 177.6(2)° in (η^2-^{i}PrNC(^{i}PrN(SiMe$_3$))N^{i}Pr)Ta(NMe$_2$)$_3$(CH$_2$Ph),[35] and 162.19(19)° in a more distorted [(η^2-^{i}PrNC(NMe$_2$)N^{i}Pr)]$_2$Ta(NMe$_2$)(=N^{t}Bu)[36]). The dihedral angle between chelate rings (N5—C9—N6) and the migrated dimethylamido groups (C16—N7—C17) in the guanidinate unit in **5** is 88.3°, which indicate negligible delocalized π interaction within the guanidinate ligand in complex **5** because the other nearly 90° dihedral angles (80.7° in (η^2-CyNC(NMe$_2$)NCy)Ta(NMe$_2$)$_4$[34] and 97.9° in (η^2-^{i}PrNC(^{i}PrN(SiMe$_3$))N^{i}Pr)Ta(NMe$_2$)$_3$(CH$_2$Ph)[35]) were also used to conclude the absence of the potential π conjugations between the p orbital of the exocyclic nitrogens and chelate NCN fragments. However, the corresponding dihedral angle (between planes of N1—C1—N1A and C9—N5—C9′A) in **6** could not be accurately determined due to the presence of the extreme disorder in this structure. In addition, the bond length of N7—C9 (1.425(4) Å) in **5** is longer than N5—C1(1.381(13) Å) in **6** and N3—C10 (1.379(5) Å) in a reported Ta(NMe$_2$)$_3$Cl[(^{i}PrN)$_2$C-NH^{i}Pr],[40] which is also longer than reported C—N bonds in the guanidinium moiety—(C$_{sp2}$—(NR$_2$)$_3^+$) 1.317−1.333 Å.[48] As a result, the less conjugated resonance structure A is believed to be the more dominant one for complex **5** (Scheme 2).

Scheme 2. Possible Resonance Structures of the Guanidinate Anion in 5 (R^3 = ^{t}Bu, R^4 = Et) and 6 (R^3 = R^4 = ^{i}Pr)

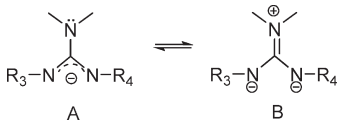

Thermal Characterization of Complexes 1−6. All complexes **1**−**6** are volatile and thermally stable enough to be purified by either vacuum distillation or sublimation and their thermal characteristics were measured by STA. (Figure 1 in the Supporting Information shows the comparison of their TGA curves with PDMAT).

The temperature of 50% mass loss derived from TGA data (T_{50}) has been demonstrated to correlate with the volatility of the sample and is used to compare relative volatilities (Table 3).[49,50] The combination of lower T_{50} with lower onset temperature derived from TGA curve is usually a strong indication of good volatility of a precursor. Clearly, complex **1** has both the lowest T_{50} (175 °C) and onset temperature (152 °C) among all four new diamides, and they are almost identical to those of PDMAT (174 and 159 °C). Our observation that both temperatures

(47) Chen, C.; Rees, L. H.; Cowley, A. R.; Green, M. L. H. *J. Chem. Soc., Dalton Trans.* **2001**, 1761.
(48) Allen, F. H.; Kennard, O.; Watson, D.; Brammer, G., L.; Orpen, A. G.; Taylor, R. *J. Chem. Soc. Perkin Trans. II* **1987**, S1.
(49) Richardson, M. F.; Sievers, R. E. *Inorg. Chem.* **1971**, *10*, 498.
(50) Li, Z.; Rahtu, A.; Gordon, R. G. *J. Electrochem. Soc.* **2006**, *11*, C787.

Table 3. STA Data of Complexes 1−6

complexes	molecular weight (g/mol)	T_{50} (°C)	onset temperature (°C)	residual mass (%)
PDMAT[a,b,c]	401.33	174	159	4.8
1[b,c]	399.31	175	153	5.4
2[b,c]	427.36	196	171	9.3
3[b,c]	413.34	190	171	5.2
4[b,c]	441.39	222	182	27
5[b,c]	527.54	190	170	1.6
6[b,c]	527.54	210	179	6.9

[a] Included for reasons of comparison. [b] Sample size: PDMAT (8.92 mg); **1** (5.15 mg); **2** (9.53 mg); **3** (12.10 mg), **4** (11.22 mg), **5** (9.56 mg), and **6** (10.57 mg). [c] All samples are liquid at their T_{50}s.

increase as the molecular mass increases (**1** ≅ PDMAT < **2** ≅ **3** < **4**) has been previously reported by other researchers, for example, the nearly linear relationship between T_{20} values and molecular weigh in ^{t}Bu derivatives of gallium chalcogenide cubanes reported by Barron et al.[51] A similar rationale cannot be applied to the two guanidinate compounds **5** and **6**, which have different T_{50} values and onset temperatures (190 and 170 °C for **5**; 210 and 179 °C for **6**) but identical molecular mass. The fact that complexes **5** and **6** bear the same molecular weight, provides a rare opportunity for us to illustrate the impact of intermolecular interactions in the solid state on the volatility of the two precursors without interference of the contribution from molecular mass. The only other direct observation of such a ligand geometry effect was proposed by Barron and his coworkers through a comparison of the relative volatility of [^{t}BuIn(μ_3-Se)]$_4$ (T_{sub} = 151 °C under 0.2 torr vacuum) and [^{n}BuIn(μ_3-Se)]$_4$ (T_{dec} = 240 °C under vacuum).[51,52] However, no further investigation along this line was conducted probably due to the instability of [^{n}BuIn(μ_3-Se)]$_4$. They attributed the deviation of the volatility from different molecular masses with regard to other ligands studied to the dispersion forces between the molecules modeled by a combination of intermolecular van der Waals interactions and the degree of branching of the alkyl ligand. In addition, Fischer and co-workers studied the influence of substituents on nitrogen in the guanidinate ligands on volatility and concluded that the variation of substituent bonded directly to the chelate ring has a greater effect than those in the exocyclic environment,[37] which is consistent with our finding here. Further, it was proposed that the intermolecular interactions between the molecules in the solid state could be the cause for the different volatilities when different moieties such as ^{i}PrNCN^{i}Pr and CyNCNCy are present, although the contribution from the difference on molecular masses can not be excluded in their studies. The packing diagrams of complexes **5** and **6** reveal that **5** has a lower order space group ($P2(1)/n$) when compared with that of **6** ($P4(2)/mbc$), whose crystallographic symmetry is greater than the molecular symmetry due to the disorder present in the molecule. However, there is no indication that one precursor packs more efficiently than the other since the densities are virtually identical (Table 1). Also, the surface of these molecules in the solid states indicates many very weak intermolecular interactions. On the basis of the aforementioned discussion, it is reasonable to speculate that the same van der Waals forces in the solid states of **5** and **6** partially induced by different major electronic resonance structures and partially by the different molecular orientations in the crystal lattice, namely the asymmetric guanidinate unit ^{t}BuNC(NMe$_2$)NEt in **5** compared to the symmetric one ^{i}PrNC(NMe$_2$)N^{i}Pr in **6**, cause the significant decrease of the T_{50} of complex **5** by 21 °C, which is also the lowest T_{50} reported for tantalum guanidinates (the T_{50}s of other tantalum guanidinates were derived from their corresponding TGA plots),[36,37] and the subsequent increase of its volatility.

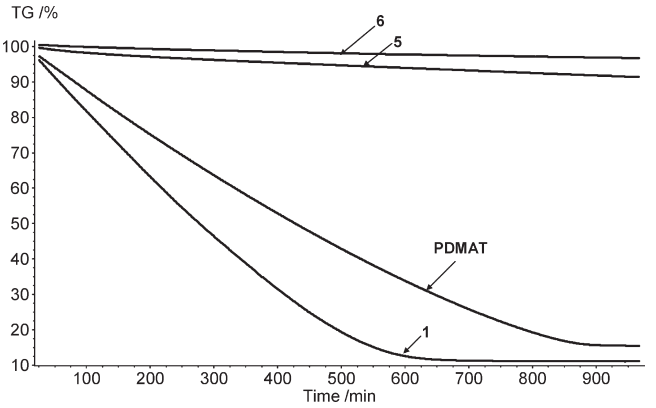

Figure 3. Isothermal TGA of **1**, **5**, **6**, and PDMAT at 80 °C (sample size: PDMAT, 12.6 mg; **1**, 12.6 mg; **5**, 11.9 mg, **6,** 12.4 mg).

To further investigate the transport properties of the two most volatile candidates—complexes **1** and **5**—isothermal TGA experiments were carried out, in which the temperature of the STA furnace was held at 80 °C for 16 h and the rates of the linear mass loss, presumably by evaporation instead of decomposition, were calculated from the TGA curves shown in Figure 3. For the purpose of comparison, the same isothermal TGA was also conducted for PDMAT and complex **6**. The fact that all DSC curves remain constant for all the samples tested verifies the assumption that only evaporation contributes to the mass loss reflected by isothermal TGA curves. Complex **1** shows the fastest mass loss rate of 20.2 μg/min (14.4 μg/min, PDMAT; 1.12 μg/min, **5**; 0.52 μg/min, **6**) at 80 °C and purged by 60 sccm Ar, which coincides with its lowest T_{50} and onset temperature and confirms its best volatility in the series. And, the higher volatility of diamide precursors over guanidinate precursors most likely arises from their lower molecular masses and suggests the future strategy for designing new volatile MOCVD/ALD precursors at a molecular level.

Regarding the thermal stability, complexes **1**−**6** are all stable up to their boiling/melting temperature and exhibit monotonic weight loss with little residual mass (<9%) remaining above 240 °C except for complex **4**, which has another gradual weight loss beyond this temperature, leaves higher residual mass (27%), but still much lower than the theoretical mass for tantalum nitride (44%) (Table 3 and Figure 1 in the Supporting Information). This indicates that even during the decomposition of the

(51) Gillan, E. G.; Bott, S. G.; Barron, A. R. *Chem. Mater.* **1997**, *9*, 796.
(52) Stoll, S. L.; Bott, S. G.; Barron, A. R. *J. Chem. Soc., Dalton Trans.* **1997**, *5*, 1315.

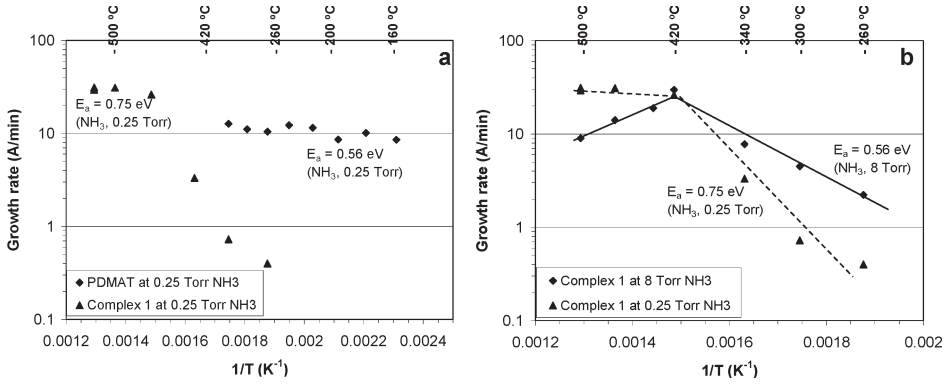

Figure 4. Arrhenius plot of log deposition rate of (a) PDMAT and complex **1** vs $1/T$ under 0.25 torr NH_3 and (b) complex **1** vs $1/T$ under 0.25 and 8 torr NH_3.

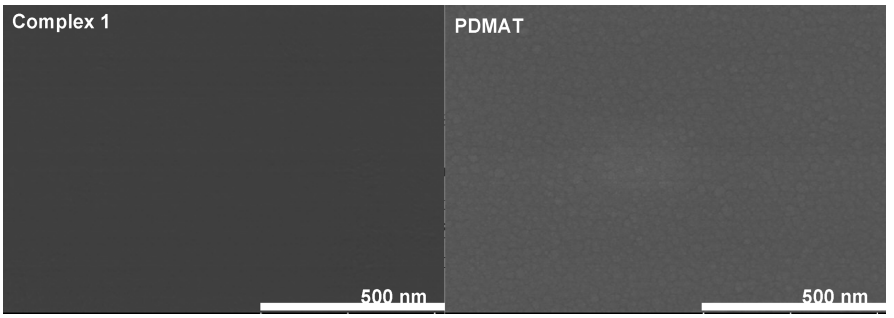

Figure 5. Top view of FESEM of Ta nitride films grown from complex **1** and PDMAT at 500 °C under 0.25 torr NH_3.

least thermally stable **4**, the extent of carbon incorporation is insignificant, which is desirable for the formation of nearly stoichiometrically pure tantalum nitride thin films. Compared to the reported Ta precursors with similar coordination numbers of nitrogens around the tantalum center, the residual mass for complex **1** (5.4%) is very close to that of the homoleptic amide, PDMAT (4.8%), and comparable to or lower than those of the newly reported hydrazido amido/imido $Ta(NMe_2)_2[(Me_3Si)NNMe_2](=N^tBu)$ (4%),[41] $Ta(NMeEt)_2[(Me_3Si)NNMe_2](=N^tBu)$ (6%),[41] and $Ta(NEt_2)_2[(Me_3Si)NNMe_2](=N^tBu)$ (20%)[41] while residual mass of amido/guanidinato **5** (1.6%) and **6** (6.9%) are lower than those reported guanidiante compounds with the ^{i}PrNCN^{i}Pr feature, $Ta(NMeEt)[\eta^2\text{-}(^i PrN)_2C(NMeEt)]_2(=N^tBu)$ and $Ta(NEt_2)[\eta^2\text{-}(^i PrN)_2C(NEt_2)]_2(=N^tBu)$ (10−12%),[36,37] and much lower than those with CyNCNCy incorporation, $Ta(NMeEt)[\eta^2\text{-}(CyN)_2C(NMeEt)]_2(=N^tBu)$[37] and $Ta(NEt_2)[\eta^2\text{-}(CyN)_2C(NEt_2)]_2(=N^tBu)$ (29−35%).[37] Coupled with their relative volatilities, complexes **1** and **5** both stand out in their individual classes, showing sufficient thermal stability and volatility to be MOCVD precursors. Between these two complexes, **1** is much more volatile and **5** is potentially more stable at high temperature, based upon all the thermal data obtained. In addition, the relatively lower residual mass and higher mass loss rate of **1** (11%, 20.2 μg/min) relative to of PDMAT (15%, 14.4 μg/min) after 16 h isothermal TGA experiments at 80 °C suggest that **1** is more thermally stable and volatile than PDMAT under the identical experimental conditions; a similar assumption could be valid under the real MOCVD conditions.

MOCVD of 1 and PDMAT. Among the five new Ta precursors presented here, complex **1** was selected for preliminary MOCVD experiments based on its volatility and thermal stability. Additionally its low melting point is beneficial for achieving constant mass transport of the precursor into the gas phase, even in a mixture of solvent vapor. MOCVD using PDMAT was also performed side by side and served as a reference for the behavior of **1** in a thin film deposition process (Table 2). Arrhenius plots of **1** and PDMAT (Figures 4), which could shed light on the transition from precursor delivery dependent, boundary-layer diffusion controlled deposition to temperature dependent, surface reaction controlled deposition, show well-defined Arrhenius behavior with a transition between surface reaction and boundary-layer controlled deposition around 420 °C for complex **1** under either 0.25 or 8 torr ammonia. The calculated activation energy for decomposition of the precursors on the substrate of interest under 0.25 torr ammonia is 0.56 eV for PDMAT (Figure 4a) and 0.75 eV for **1** (Figure 4a) according to the Arrhenius equation ($k = Ae^{-E_a}/RT$, $A = 8.623 \times 10^{-5}$). This further indicates that **1** is a more stable tantalum nitride precursor from the viewpoint of avoiding gas-phase interactions with coreactants, particularly if there is a risk of backdiffusion of coreactants toward the vaporization system.

SEM images of Ta nitride films from both complex **1** and PDMAT (Figure 5) deposited under the same process conditions (500 °C under 0.25 Torr ammonia) show smooth and comparable morphology without obvious agglomeration. Films deposited from both precursors

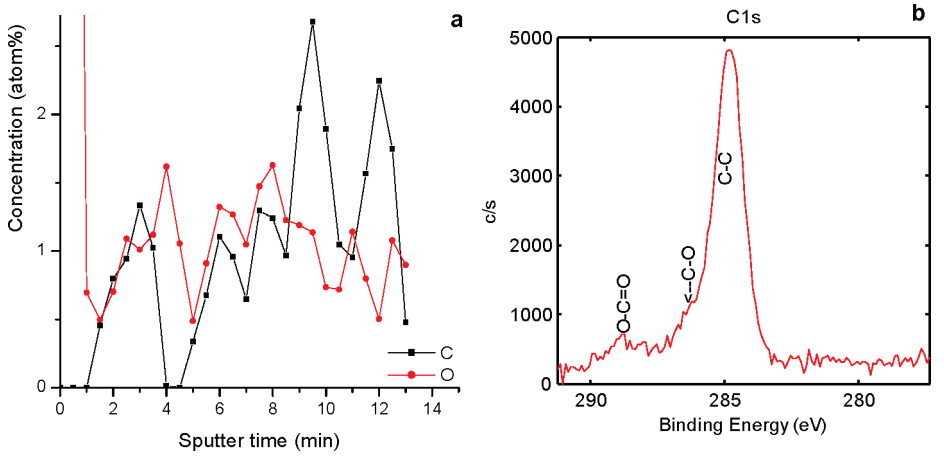

Figure 6. XPS spectra of tantalum nitride film deposited at 500 °C under 0.25 torr NH_3 using complex **1**. (a) Theoretical fit to the experimental data. (b) Depth profile based on the fits to the data.

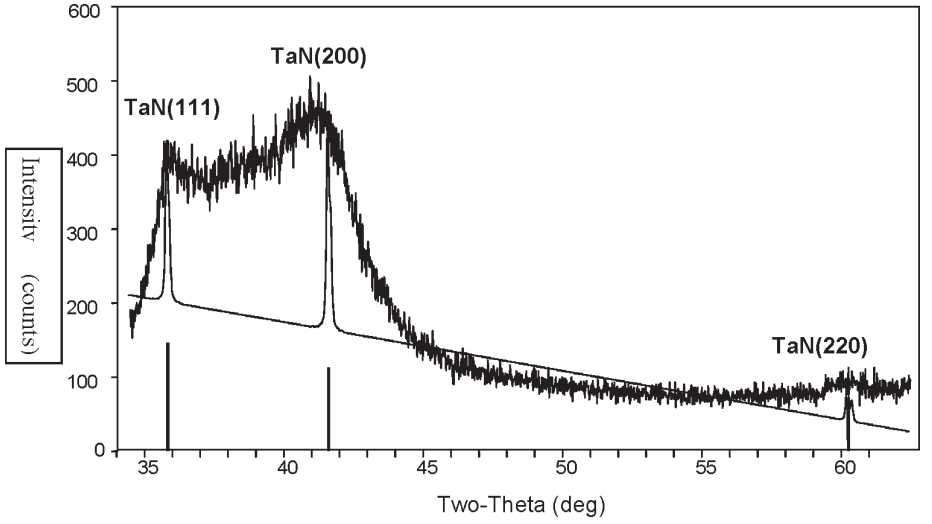

Figure 7. XRD spectra of tantalum nitride film deposited at 500 °C under 0.25 torr NH_3 using complex **1**. Theoretical fit to the experimental data is shown in a solid curve, and the reported diffraction patterns for cubic TaN (111), (200), and (222) planes (JCPDS 49-1283) are labeled in vertical solid lines.

passed the tape test using an ASTM international method, indicating relatively good robustness and adhesion properties. RBS analysis (see Figure 2a and b in the Supporting Information) showed the composition of the deposited tantalum nitride film from complex **1** at 500 °C under 0.25 torr ammonia being $TaN_{1.22\pm0.14}$ with both carbon and oxygen levels below the detection limits of RBS (< 5 at.%), which falls into the reported compositions of the cubic TaNx phase ($x = 0.9-1.3$).[16,54] An XPS depth profile was used to confirm the low carbon (average 1.1 at %) and oxygen (average 1.0 at %) levels of the as-deposited $TaN_{1.22\pm0.14}$ films in an analysis depth of ~50−100 Å (Figure 6a). XPS detection limits of these elements in TaN are 0.5−1 at %. Furthermore, the observed C_{1s} region of the as-deposited $TaN_{1.22\pm0.14}$ film only shows the signal at 285 eV assigned to the organic carbons arising from the sputtering process in the XPS experiment itself (Figure 6b). No visible carbidic carbon signal is present, which is usually below 285 eV binding energy.[12] This again confirms the nearly carbon free as-deposited $TaN_{1.22\pm0.14}$ films from **1**. In addition, N_{1s} binding energy (397.4 eV) agrees with reported values of 397.5 eV in stoichiometric TaN.[10,23] Broad XRD peaks were obtained for the tantalum nitride film grown at the highest accessible substrate temperature (500 °C) on our CVD tool using complex **1** and with theoretically fitted X-ray diffraction features assigned to cubic tantalum nitride (111), (200), and (220) planes inconclusively based on standard card patterns for cubic tantalum nitride powder (Figure 7). Such poorly distinguished XRD peaks are not unusual in the MOCVD of tantalum nitride thin films at substrate temperatures below 500 °C, and broad XRD peaks of cubic tantalum nitride films deposited by MOCVD at 500 °C using $(Et_2N)_3Ta(=N^tBu)$ (TBTDET)[12] and amorphous tantalum nitride films deposited below 650 °C using $[Ta(NMeEt)[\eta^2\text{-}(^i PrN)_2C\text{-}(NMeEt)]_2(=N^tBu)$[13] have been observed previously. Resistivity of the TaN films were calculated from the measured

(53) Winter, C. H.; Jayaratne, K. C.; Proscia, J. W. *Mater. Res. Soc. Symp. Proc.* **1994**, *327*, 103.
(54) Shin, C.-S.; Kim, Y.-W.; Gall, D.; Greene, J. E.; Petrov, I. *Thin Solid Films* **2002**, *402*, 172.

sheet resistances and film thicknesses determined by wavelength dispersive XRF. The $TaN_{1.22\pm0.14}$ films deposited at 500 °C under 0.25 torr ammonia using **1** has a resistivity of 1.4×10^3 $\mu\Omega$ cm, comparable to 1.2×10^3 $\mu\Omega$ cm of films deposited using PDMAT under the same process condition. These resistivities are in line with those of $TaN_{1.5}H_{0.3-0.5}$ films deposited at 340 °C using $Ta(NEt_2)_2(NCy_2)_2$ (2.5×10^5 $\mu\Omega$ cm),[10] cubic tantalum nitride deposited above 400 °C using $[TaCl_2(NNMe_2)(NHNMe_2)(NH_2NMe_2)]_2$ (2.5×10^5 $\mu\Omega$ cm),[53] cubic and nearly stoichiometric TaN films deposited at 600−650 °C using TBTDET (9.0×10^2−2.0×10^3 $\mu\Omega$ cm),[12] and films deposited at 500−800 °C using [Ta(NMeEt)[η^2-(^{i}PrN)$_2$-C(NMeEt)]$_2$(=N^{t}Bu) (7.0×10^3−1.5×10^4 $\mu\Omega$ cm)[13,36] but well below reported resistivity of Ta_3N_5 films (10^6 $\mu\Omega$ cm) grown at 400 °C from PDMAT.[9] Further optimization of the process parameters such as deposition temperature, substrate type, plasma-enhancement, ammonia pressure, and postdeposition annealing could potentially make the films purer, more stoichiometric, and their resistivity closer to that of bulk cubic tantalum nitride (2.0×10^2−3.0×10^2 $\mu\Omega$ cm) for advanced barrier applications.[55,56]

Conclusions

The modifications of homoleptic tantalum amide, PDMAT, via two alternative chelate approaches - incorporations of diamide ligands and insertion of the carbodiimide moiety, yielded five new precursors **1**−**5** with promising thermal properties. Complex **1** is a low melting point solid at room temperature, can be purified by vacuum distillation at large scales (> 200 g), and shows enhanced thermal and chemical stability while preserving the volatility when compared to commercially available PDMAT. Furthermore, complex **5** exhibits better thermal properties when compared to all the guanidinate precursors reported to date and demonstrate the impact of ligand geometry in the solid state on the volatility.[36,37] The difference between **1** and **5** with respect to thermal characteristics could shed light on the future directions of designing CVD/ALD precursors by keeping the molecular masses low and tuning electronic and steric aspects of the ancillary ligands for different film applications. Finally, MOCVD tantalum nitride thin films were successfully grown using **1** and extensively characterized. The nearly carbon- and oxygen-free and stoichiometric as-deposited films with similar morphology and resistivity to those using PDMAT show good promise of **1** becoming an alternative MOCVD/ALD precursor for tantalum nitride application.

Acknowledgment. We thank Drs. Philip S. Chen and Bryan Hendrix at ATMI for assistance on XRD measurement and film adhesion testing. We also would like to extend our thanks to the Paul and Wilma Ziegler Professor of Chemistry - Ziling (Ben) Xue and Drs. Xianghua (Bruce) Yu and He (Steve) Qiu at the University of Tennessee, Knoxville, for their attempted efforts to determine the structure of complex **1**.

Note Added after ASAP Publication. Due to a production error, this paper published ASAP November 25, 2009 with errors throughout the text; the corrected version published ASAP December 7, 2009.

Supporting Information Available: Crystallographic information files (CIF). This material is available free of charge via the Internet at http://pubs.acs.org.

(55) Hieber, K. *Thin Solid Films* **1974**, *24*, 157.
(56) Call, T. In *Carbide Nitride and Boride Materials Synthesis and Processing*; Weimer, A. W., Ed.; Chapman and Hall: New York, 1997.